Determination of Important Contact Parameters for Spur Gear Design

Getachew Admassie Ambaye

Faculty of Mechanical and Industrial Engineering, Bahir Dar Institute of Technology (BiT), Bahir Dar, Ethiopia
gecheadmassie@gmail.com

Abstract. This study focused on the determination of the important contact parameters of spur gear design for the investigation of different parametric studies such as the maximum pressure, contact width, contact film thickness, sliding velocities, and others. The single and double tooth contact region has been determined for the given gear parameters along with their contact lengths. The contact width and pressure can be determined by considering the engaged spur tooth as a cylindrical object. The film thickness will vary from the mesh approach (minimum) to the mesh recesses (maximum). The film thickness is decreased in a single tooth contact region a maximum value at the mesh termination.

Keywords: Sliding velocity, contact width, contact pressure, film thickness

1 Introduction

The motion and power are transmitted through a successive contact of gear tooth surfaces. The gear mates have a maximum of two teeth in contact this is called contact ratio, and the distance from one contact pair of gear to the other contact gear tooth pair is called contact length. In simple expression, the contact length is an imaginary line that passes through pitch point from the mesh initiation to mesh termination points.

The load is distributed through the contact length of the gear, which has a strong influence on the performance of the gear. The gear with a longest contact length has less chance to fail early than the gear with the shortest contact length unless manufacturing and other situations affect the system. To illustrate this, the spur gear has the shortest contact length than helical gear, therefore, the spur gear can fail early than helical gear if both gears subjected to same load and operating conditions. In this section the length of mesh initiation and termination, contact ratio, surface and sliding velocity of the gear will be determined. Figure 1 shows the length of contact, recess and approach angles for a mesh. The length from point A to C and from C to E is called the length of mesh initiation (approach) and length of mesh termination (recess) respectively [1]. A single gear tooth contact will show between a point B to D, while in a length between A to B and D to E double tooth contact will occur. The full mesh cycle can be acquired by summing up the roll angle approach and termination

angles. In other wards point, B and D are called the Lowest point of single tooth contact (LPSTC) and the highest point of single tooth contact (HPSTC) respectively.

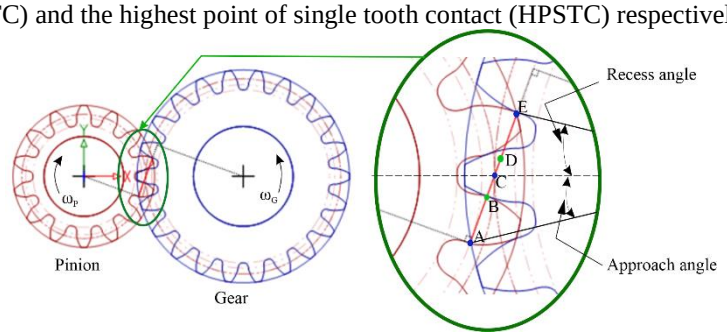

Fig. 1. 2D Model of spur gear [1].

Wang et al. [2] investigated a novel numerical model with high computational accuracy for rough surface contact is developed and applied to the wear prediction of spur gears. There are a number of researches have been studied to in investigate and compare the numerical contact patterns with the existing and novel model [3-5].

Getachew and Hirpa [6] investigated the transmission error and mesh time varying stress of the spur gear by determining the contact parameters of the same specification that have been used for this study. The effect of backlash on the flash and contact temperature of the spur gear is studied [1]. Nordin and Gutman investigated the conrolo mechanism of backlash [7]. The performance of the gear can be determined by the amount of transmission error, time varying mesh stiffens and other [8-10]. Numerical methods are commonly used to determine the transmission error and other performance parameters of the dynamic system [11, 12].

The gear fails due to an excessive deformation and continuous wear due to fatigue by depleting the gear tooth thickness and the contact width [13, 14]. This paper will have revealed how the contact parameters of the spur gear is determined for different parametric studies by taking a specific gear design as a case study.

2 Contact length and rolling angles

The length of meshing initiation is the distance from the beginning of contact until the point of contact arrives at the pitch point, While the length of mesh termination is the distance from the pitch point to the end of contact arrives at the point and it is calculated as -9.327 mm and 8.638 mm respectively using Equation 1 (a) and (b).

$$S_i = -\sqrt{(r_{aG}^2 - r_{bG}^2)} - r_G \sin\alpha \qquad (1a)$$

$$S_t = -\sqrt{(r_{aP}^2 - r_{bP}^2)} - r_P \sin\alpha \qquad (1b)$$

The other important parameter is the rolling approach angle and angle of termination. Roll approach angle is the angle between the horizontal line and the line that begin from center of rotation and passes through the mesh initiation point. While, recess roll

angle is the angle between the horizontal line and the line that begin form center of rotation and pass through the mesh termination point. These both parameters can be determined from the Equations 2 (a) and (b) as 12.93° and 18.81°.

$$\varphi_i = -\frac{S_i}{r_{bG}} \tag{2a}$$

$$\varphi_t = -\frac{S_t}{r_{bP}} \tag{2b}$$

Length of line of action is the sum of length of mesh initiation and termination and is given by Equation 3, and it is calculated as 17.965 mm.

$$l = S_i + S_t \tag{3}$$

The contact ratio is given by Equation 4. A contact ratio of 1 means that only one tooth pair is engaged at all times during the course of action. The gear tooth may not carry the load as good as the gear tooth that there are more than one pair of tooth contact, this is undesirable because slight errors in the tooth spacing will cause oscillations in the velocity, vibration, and noise. For the satisfactory performance of power transmitting gears, a value of 1.4 is used as a practical minimum. A lower contact ratio also necessitates a higher degree of accuracy in meshing to ensure quiet running of the gear set, but from Equation 4 the contact ratio is 1.52 and this indicates that one pair of teeth are always in contact, and the second pair of teeth are in contact 52% of the time Norton et al. [15].

Low-contact-ratio spur gears suffer from abrupt changes in the transmitted load because of the continuous engagement and disengagement of teeth in a meshing cycle. These changes generate noise and vibrations, resulting in poor lubrication and increased tooth wear, and can even cause tooth breakage.

$$M_c = CR = \frac{l}{P_b} \tag{4}$$

From Figure 1, it is shown that a single tooth contact is occurred between points B and D. This indicates that the single tooth contact starts at length AB (S1) and ends at length AD (S2) from mesh initiation (point A). The pitch point (C) can be taken as a reference and then the length along the right side of this can be considered as a positive and along the left side negative. These distances, S1 and S2 can be calculated by:

$$S_1 = \frac{S_i + (M_c - 1)S_t}{M_c} \tag{5a}$$

$$S_2 = \frac{S_i(M_c - 1) + S_t}{M_c} \tag{5b}$$

From the above equation S1 = -3.18 mm and S2 = 2.49 mm. In other word, there is a single meshing pair when -3.18 mm < S < 2.49 mm, and there are a two meshing pairs when the meshing position is in the range of Si ≤ S ≤ S1 or S2 ≤ S ≤ St. Point S1 and S2 along the line of action are called the lowest point of single tooth contact and the highest point of single tooth contact respectively.

3 Surface velocity and sliding velocity

The center of the gear is constrained and subjected to a constant rotational load. The surface velocity will vary from the beginning of mesh to mesh termination due to the length from the center of the rotational axis along line of action. Radii of the two equivalent cylinders at a given meshing position are given by

$$R_{P,G} = r_{P,G} \sin\alpha \pm S \tag{6}$$

The equivalent radius of the elastohydrodynamic lubrication (EHL) contact is given by:

$$R'(S) = \frac{(R_P R_G)}{(R_P + R_G)} = \frac{(r_P \sin\alpha + S)(r_G \sin\alpha - S)}{c \sin\alpha} \tag{7}$$

The surface velocities of the two cylinders are given by

$$U_{P,G}(S) = \omega_{P,G} R_{P,G} \tag{8}$$

The entraining velocity of the EHL contact

$$U(S) = \frac{U_P + U_G}{2} = \omega_P r_P \sin\alpha + \frac{(\omega_P - \omega_G)S}{2} \tag{9}$$

Sliding velocity is the relative velocity in a transverse plane of a common contact point between mating gear teeth and is given by Equation 10.

$$U_S(S) = U_P - U_G = (\omega_P + \omega_G)S \tag{10}$$

The geometric parameters and operational conditions of spur gears used for this study are based on parameters used in Taburdagitan and Akkok [16]. These parameters and the related operational conditions are given in Table 1.

Table 1. Geometric parameters and operational conditions of the meshing gear pair

Parameter (symbol)	Value
Module (m)	4 mm
Pressure angle ($\boldsymbol{\alpha}$)	20°
Number of teeth, pinion ($\boldsymbol{Z_P}$)	14
Number of teeth, gear ($\boldsymbol{Z_G}$)	22
Face width (B)	6 mm
Load per unit face width (w)	75.5 N/mm
Angular velocity of pinion ($\boldsymbol{\omega_P}$)	2090 rpm

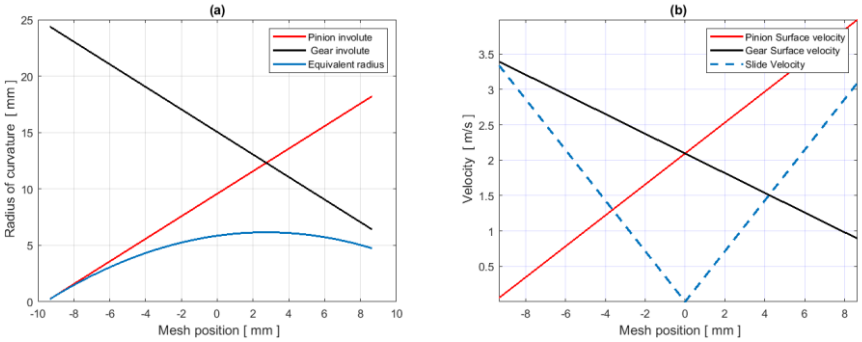

Fig. 2. Gear (a) radius of curvature and (b) velocities of gear.

The radius of the curvature of the involute of gear tooth for both pinion and gear is shown in Figure 2 (a). The figure illustrates that the radius of curvature of pinion gear tooth is minimum at the mesh initiation and increased to the maximum value as it is shown in the figure, on the other hand, the radius of curvature of the gear involute tooth is maximum at the mesh initiation and decrease to the minimum value at the mesh termination. The pinion and gear radius of curvature is equal at 2.85 mm mesh position along the line of action. The equivalent radius of curvature also shown in the figure and it increases gently from mesh initiation till it reaches to the point where the pinion and gear have the same radius of curvature and then it starts to decrease gently, it has a downward parabolic shape. These radii of curvatures are used to determine the surface and sliding velocities of the gear. The contact of the gear tooth shows a rolling and sliding velocities. Both surface velocities for pinion and gear and sliding velocities are shown in Figure 2 (b). The surface velocity of the pinion is increased from 0.2 m/s to a maximum value of 4 m/s, this indicates that the radius of involute at the mesh initiation is very small and as it goes from this point it increases [1]. The surface velocity of the gear is maximum as mesh initiation and decrease to 0.8 m/s at the mesh termination point. In addition, at the pitch point the surface velocities of pinion and gear are the same, in other words there is a pure rolling at the pitch circle.

4 Contact width and contact stress

In mechanical engineering and tribology, Hertzian contact stress is a description of the stress between mating parts. Theoretically, the contact area of two spheres is a point, and it is a line for two parallel cylinders. As a result, the contact pressure between two curved surfaces should be infinite for both of these two cases, which will cause immediate yielding of both surfaces.

However, a small contact area is being created through elastic deformation in reality due to deformation at the contact surfaces. Figure 3 shows the Hertz contact components of sectional two elastic objects for general cases. When the contacting components are subjected to a load there is a point contact and then as the load increases the stress induced in the contacting bodies increases and as a result, the contacting area

will grow as an elliptical shape. The maximum contact pressure, Pmax is found at the center and it decreases as it goes away from the center. The contact width, b is measured from the semi-minor axis of the elliptical geometry as shown in the graph.

The gear tooth has a cylindrical shape and the Hertz contact theory can be applied. Conjugate action of gear teeth in mesh consists primarily of sliding and rolling motions. At the pitch line, sliding velocity is zero; however, sliding velocity increases when the conjugated tooth contact line travels away from the pitch line in both directions. The contact pressure of gear teeth in mesh also changes along the line of action. In this study cylindrical contact object is considered for the analysis of spur gear contact width and pressure.

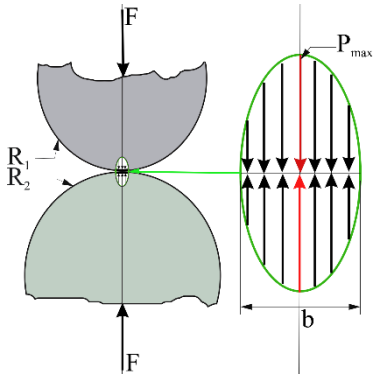

Fig. 3. Contact between two sectioned cylinders, general case

4.1 Contact width

Contact width is used to determine the contact pressure of mating pairs. Contact width is given by Equation 11, and it shows that it is directly proportional to the equivalent radius of curvature and inversely proportional to the equivalent elastic of module. Equivalent radius is calculated in the previous Section, Equation 7, it varies along the line of action. The equivalent modulus is given by Equation 12, in this thesis report the both mating components of gear have the same modulus of elasticity as given in Table 2. Both gear and pinion are made from steel SAE-AISI 1045 at 20 ºC.

$$b = \sqrt{\frac{8WR'}{\pi E'}} \tag{11}$$

$$\frac{1}{E'} = \frac{1}{2}\left[\frac{1-\nu_P^2}{E_P} + \frac{1-\nu_G^2}{E_G}\right] \tag{12}$$

Table 2. Material properties of the steel SAE-AISI 1045 at 20***ºC*** [14].

Parameter	Value
Mass density,$\boldsymbol{\rho}$	$7.86 \times 10^{-6}\ Kg/mm^3$
Modulus of Elasticity, $\boldsymbol{E_P}$ & $\boldsymbol{E_G}$	$207 \times 10^{3}\ N/mm^2$
Poisson ratio,$\boldsymbol{\nu}$	0.3

Specific heat, C_P	$485 \times 10^3 (Nmm)/Kg℃$
Thermal conductivity, κ	$42.3\ (Nmm)/mm℃$

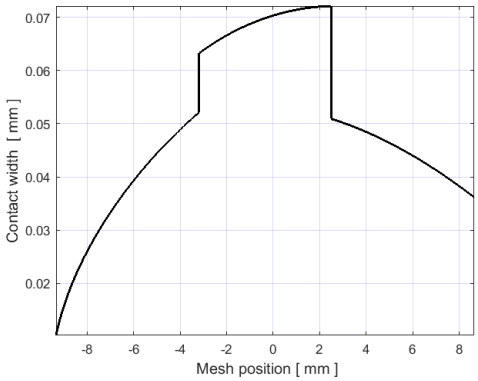

Fig. 4. Contact width.

Figure 4 shows that the contact width increased from the point where the meshing of gear sets start to the LPSTC, and the maximum contact width has occurred at HPSTC 0.073 mm, and at mesh termination point the contact width is around 0.0375 mm. The contact width is maximum under single tooth contact, i.e between - 3.18 to 2.49 mm. This shows that the contact width is maximum under the single tooth contact region.

The gear width is proportional to the load that applied on the gear, the load is shared into two teeth in the double tooth contact region. Near to the pitch point, the width is maximum. This is because the gear load is carried by a single tooth only, this indicates that, the more the load subjected the more the deformed width will be produced. Once the gear width is determined the maximum contact pressure can be determined, and this show in the next section.

4.2 Contact pressure

The contact stresses on the gear surfaces can be estimated by analytical equations based on the frictionless elastic theory developed by Hertz in 1881 [17]. The gear contact is analyzed with the assumption that the contact is between two cylinders with radii equal to the radius of the curvature of the teeth. The contact geometry between the two elastic contact bodies in general cases is as shown in Figure 4.3. The Hertz equations can be utilized to calculate the contact pressure at the tooth surfaces of two mating spur gears.

The contact pressure is the ratio of the normal load to the true contact area. Contact stress is generally the deciding factor for the determination of the required dimensions of gears. The maximum and average contact pressure of the two cylindrical contact bodies is given by Equation 13 (a) and (b). In this thesis the maximum pressure is calculated as shown in Figure 5.

$$P_{max} = \frac{2W}{\pi b} \tag{13a}$$

$$P_{average} = \frac{W}{4b} \tag{13b}$$

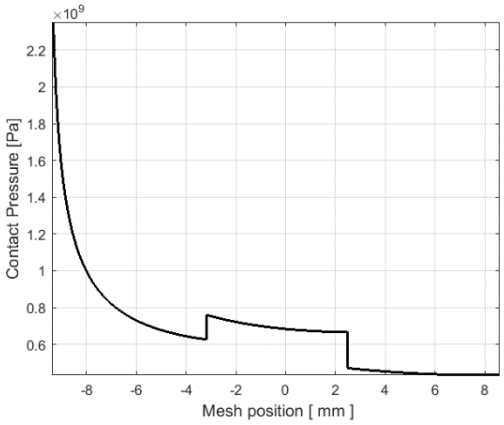

Fig. 5. Maximum contact pressure.

As shown in Figure 5, the maximum contact pressure (2.4 GP a) is obtained around the tip of the gear tooth, and it decreases gently to 610 MP and at the LPSTC region, and then it increases to 780 MP a without change of mesh position, and then it decreases gently to a point HPSTC region which is almost 680 MP a. and then the minimum contact pressure is occurred at the mesh termination which is almost 500 MP a. If the gear tooth profile is modified the maximum contact pressure will occur on a single tooth, contact region. Maximum contact pressure is occurred at the LPSTC and then decreases gently to the point of HPSTC.

In this paper the important contact parameters have been determined. The radius of involute is used to determine the sliding velocity of the gear, and the equivalent radius of curvature is maximum at above pitch point. The sliding velocity of the spur gear is maximum at the mesh initiation and decreases and eventually it gets zero at the pitch point and it increases again. The other main point of this paper is it's about the contact width and pressure, the cylindrical contact bodies have been considered to analyzed the gear contact width and maximum pressure. Maximum contact width is found on the single tooth contact region. The maximum contact pressure is maximum at the mesh initiation and it decreases gently until it reaches on the LPSTC region. The maximum contact pressure can be found on the single tooth contact region if the tip of the gear tooth is modified.

5 Minimum film thickness

The oil plays a significant role on the performance of the rotating mechanical components. The temperature of the oil will greatly influence the failure and performance of the gear [18]. Lubrication regimes are basic contact conditions that predict the way

the load is carried from one surface to another of contacting bodies. There are four main lubrication regimes that are commonly known.

Hydrodynamic lubrication: the contacting bodies are separated by a liquid lubricant which is thick enough to avoid any direct contact between their surfaces. The load is then carried by the pressurized lubricant and it is shown in Figure 6 (a). The thickness of the film (h) can lead in to another division, if $\boldsymbol{h \geq 0.25\ \mu m}$ is called a hydrodynamic lubrication (HDL) regime, while if $\boldsymbol{0.025 \geq h \leq 5\ \mu m}$ we call it elasto hydrodynamic lubrication (EHL) regime.

Mixed lubrication (ML): the average lubricant film thickness between contacting bodies is lower than the mean roughness of their surfaces. Direct contacts occur between asperities. The load is then carried partly by the lubricant, partly there is a direct contact between mating pairs as shown in Figure 6 (b).

Boundary lubrication (BL): No liquid lubricant is used: the load is carried by direct contact between bodies at the level of the asperities, this is shown in Figure 6 (c), the thickness of the film is between 1 and 3 ***nm***.

Solid-film lubrication: the contacting bodies are separated by a solid lubricant thick enough to avoid any contact between the tool and the work piece. Figure 6 (d) shows that the load is fully carried by the solid lubricant.

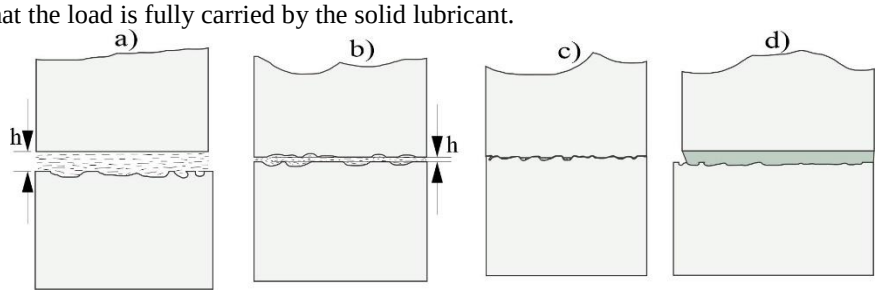

Fig. 6. Lubrication regimes (a) HDL, (b) ML, (c) BL and (d) Solid-film lubrication.

There are a number of studies that focuses on the determination of the film thickness and related gear parameters such as the stiffens and others [19-21].

The exact analysis of elastohydrodynamic lubrication by Hamrock and Dowson, provided the most important information about EHDL [22]. Film thickness at each meshing position is expressed in Equation 14:

$$h_o = 3.068 C_P C_T R' U^{0.69} g^{0.56} W_F^{-0.1} \quad (14)$$

Compressibility reduction factor CP and inlet shear heating reduction factor respectively CT can be calculated by the equations that given in the nomenclature.

The lubricant pressure viscosity (ψ) and temperature viscosity (β) factors respectively. These and other parameter values are given in the Table 3.

Table 3. Lubricant parameter [22]

Independent parameters	Value
Lubricant ambient temperature, $\boldsymbol{T_o}$	100℃
Lubricant ambient viscosity, $\boldsymbol{\eta_o}$	$0.01\ Pa\ s$
Pressure viscosity coefficient, $\boldsymbol{\psi}$	$1.2 \times 10^{-8}\ Pa^{-1}$

Temperature viscosity coefficient, $\boldsymbol{\beta}$	$0.04°C^{-1}$
Lubricant thermal conductivity,$\boldsymbol{K_f}$	$0.14\ W/(m°C)$
Lubricant density, $\boldsymbol{\rho_f}$	$800\ kg/m^3$
Lubricant specific heat, $\boldsymbol{C_f}$	$2290\ J/(kg°C)$

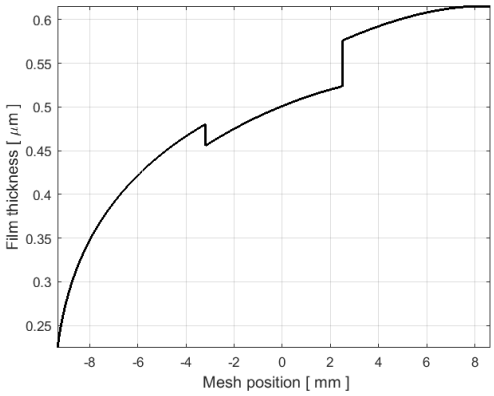

Fig. 7. Film thickness.

Figure 7 shows that the film thickness increases from mesh initiation to LPSTC exponentially, then minimum film thickness is found at the mesh initiation and which is around 0.2 µm. The film thickness is decreased in a single tooth contact region and increases smoothly up to HPSTC region, and then it increases exponentially to 0.62 µm at the mesh termination. The minimum film thickness at mesh initiation can be altered by modifying the gear tooth profile, this will make the minimum film thickness lay between LPSTC and HPSTC region. In general, the minimum film thickness is found in single tooth contact region.

Conclusion

This paper summarized the contact parameters of the spur gear for some specific gear specifications. Determinations of these parameters will pave the way to investigate different parametric studies of the spur gear. The sliding velocity at the pitch point is zero, it indicates that the gear is taking a pure rolling motion at the pitch points. However, a slight movement from this point will yield both the rolling and sliding motions. To study the contact width and pressure of the gear tooth, it's essential to consider the gear tooth as a cylindrical object coming in contact. Therefore, the contact shape will give an elliptical deformed shape and the maximum contact width is obtained between the single tooth contact region. The film thickness is increased parabolic from the mesh initiation to the single tooth contact point and it reduces and it again increases parabolic after the last point of the single contact point. This paper has been wide up to the determination of the contact parameters of the spur gear.

References

1. Ambaye, G., Lemu, H., Numerical Study of Effect of Backlash on Flash Temperature of Spur Gear, (2020) *International Review of Mechanical Engineering (IREME)*, 14 (11), pp. 684-692. doi:https://doi.org/10.15866/ireme.v14i11.19763
2. Wang, H., Zhou, C., Wang, H., Hu, B. and Liu, Z., 2021. A novel contact model for rough surfaces using piecewise linear interpolation and its application in gear wear. *Wear*, p.203685.
3. Marciniec, A., Pacana, J., Pisula, J.M. and Fudali, P., 2018. Comparative analysis of numerical methods for the determination of contact pattern of spiral bevel gears. *Aircraft Engineering and Aerospace Technology*.
4. Hu, Z., Ding, H., Peng, S., Tang, Y. and Tang, J., 2019. Numerical determination to loaded tooth contact performances in consideration of misalignment for the spiral bevel gears. *International Journal of Mechanical Sciences*, *151*, pp.343-355.
5. Sekar, R.P., 2019. Determination of load dependent gear loss factor on asymmetric spur gear. *Mechanism and Machine Theory*, *135*, pp.322-335.
6. Ambaye, G.A. and Lemu, H.G., 2020, October. Effect of backlash on transmission error and time varying mesh stiffness. In *International Workshop of Advanced Manufacturing and Automation* (pp. 18-28). Springer, Singapore.
7. Nordin, M. and Gutman, P.O., "Controlling mechanical systems with backlash a survey," *Automatica*, vol. 38, no. 10, pp. 1633–1649, 2002.
8. Zhou, W., Zhu, R., Liu, W. and Shang, Y., 2021. An Improved Dynamic Transmission Error Model Applied on Coupling Analysis of Gear Dynamics and Elastohydrodynamic Lubrication. *Journal of Tribology*, *144*(5), p.051601.
9. Wang, J., Liu, N., Wang, H. and Guo, L., 2021. Nonlinear dynamic characteristics of planetary gear transmission system considering squeeze oil film. *Journal of Low Frequency Noise, Vibration and Active Control*, *40*(2), pp.823-851.
10. Shi, J.F., Gou, X.F. and Zhu, L.Y., 2020. Calculation of time-varying backlash for an involute spur gear pair. *Mechanism and Machine Theory*, *152*, p.103956.
11. Rahmani , H., Moslemi Petrudi, A., & Cristian Scurtu , I. . (2021). Numerical Analysis and Simulation of RM12 turbofan rotor system. *Technium Romanian Journal of Applied Sciences and Technology*, *3*(1), 51–60. Retrieved from https://techniumscience.com/index.php/technium/article/view/2536
12. M. H. K., Amin Moslemi Petrudi, & Ionut Cristian Scurtu. (2020). One-Dimensional Analysis and Modeling of the Xu 7 Engine Due to Changes in Valve Timing to Improve Engine Performance. *Technium Romanian Journal of Applied Sciences and Technology*, *2*(4), 46–53. https://doi.org/10.47577/technium.v2i4.1036
13. Benaïcha, Y., Perret-Liaudet, J., Beley, J.D., Rigaud, E. and Thouverez, F., 2022. On a flexible multibody modelling approach using FE-based contact formulation for describing gear transmission error. *Mechanism and Machine Theory*, *167*, p.104505.
14. Liu, H., Liu, H., Zhu, C. and Tang, J., 2020. Study on gear contact fatigue failure competition mechanism considering tooth wear evolution. *Tribology International*, *147*, p.106277.
15. Norton, R.L. and Han, J., *Design of machinery*. Higher Education Press, 2007.
16. Taburdagitan, M. and Akkok, M., "Determination of surface temperature rise with thermoelastic analysis of spur gears," *Wear*, vol. 261, no. 5-6, pp. 656–665, 2006.
17. Liang, X., Zuo, M.J. and Feng, Z., "Dynamic modeling of gearbox faults: A review," *Mechanical Systems and Signal Processing*, vol. 98, pp. 852–876, 2018.
18. Höhn, B.R. and Michaelis, K., 2004. Influence of oil temperature on gear failures. *Tribology International*, *37*(2), pp.103-109.

19. Amarnath, M., Sujatha, C. and Swarnamani, S., 2009. Experimental studies on the effects of reduction in gear tooth stiffness and lubricant film thickness in a spur geared system. *Tribology international*, *42*(2), pp.340-352.
20. Hamel, M., Addali, A. and Mba, D., 2014. Investigation of the influence of oil film thickness on helical gear defect detection using Acoustic Emission. *Applied acoustics*, *79*, pp.42-46.
21. Jian, G., Wang, Y., Zhang, P., Xie, Y. and Zhao, J., 2020. Analysis of lubricating performance for involute spur gear under vibration. *Lubrication Science*, *32*(7), pp.344-357.
22. Chang, L., Jeng, Y.R. and Huang, P.Y., "Modeling and analysis of the meshing losses of involute spur gears in high-speed and high-load conditions," Journal of Tribology, vol. 135, no. 1, 2013.
23. Halim Dwi Putra, Decoding Consumer Choices: Navigating The Impact Of Zero Moment Of Truth On Buying Decisions In Bengkalis Island, Jurnal Ilmiah EDUNOMIKA, ISSN 2598-1153, Vol 8, No 2 (2024), DOI: http://dx.doi.org/10.29040/jie.v8i2.12244

24. Nita, C. M., Bocanete, P., & Scurtu, I. C. (2022). Experimental methods for determining the characteristic quantities of unconventional naval propellers. Technium: Romanian Journal of Applied Sciences and Technology, 4(8), 56–63. https://doi.org/10.47577/technium.v4i8.7265

25. Nair, S., Shetty, A., Maurya, N., & Scurtu, I. C. (2021). Effective Techniques for Wireless Charging for Unmanned Aerial Vehicles (UAV). Technium: Romanian Journal of Applied Sciences and Technology, 3(1), 128–137. Retrieved from https://techniumscience.com/index.php/technium/article/view/2514

26. Romeo Boşneagu, Andra-Teodora Nedelcu, Ionut Cristian Scurtu, Black Sea-the geopolitical, economic, social and military importance, Journal of Physics: Conference Series, Vol. 1122, Pages 012006

27. Gulpinar, F.; Balikci, A. Driving Asynchronous Induction Launchers: Design and Simulation of a Novel Power Conditioner with a Brief Review. Energies 2022, 15, 9360. https://doi.org/10.3390/en15249360

28. F. Gulpinar and A. Balikci, "Design and Implementation of a Novel Power Conditioner for Linear Induction Launchers," 2020 International Conference on Electrical, Communication, and Computer Engineering (ICECCE), Istanbul, Turkey, 2020, pp. 1-4, doi: 10.1109/ICECCE49384.2020.9179350.

29. Gülpınar, F., Sarı, F., and Uzun, Y. (2017) Analysis of a Novel Four Level Flying Capacitor H – Bridge
Converter. International Journal of Renewable Energy Development, 7(1), 71-75. https://doi.org/10.14710/ijred.7.1.71-75

Nomenclature

$$C_P = \left(1 + \frac{0.58 \times 10^{-9} \quad P_{max}}{1 + 1.68 \times 10^{-9} P_{max}}\right)^{-1}$$

$$C_T = \exp\left(-0.75\beta \frac{\eta_o u^2}{4k_f}\right)$$

$$u = \frac{U_P + U_G}{2}$$

$$U = \frac{\eta_o u}{E'R'}$$

$$g = \psi E'$$

$$W_F = \frac{\omega}{E'R'}$$